Photonic-crystal-fiber-enabled micro-Fabry–Perot interferometer

Joel Villatoro,[1,*] Vittoria Finazzi,[1] Gianluca Coviello,[1] and Valerio Pruneri[1,2]

[1]*ICFO–Institut de Ciencies Fotoniques, Mediterranean Technology Park, 08860, Castelldefels, Barcelona, Spain*
[2]*ICREA–Institucio Catalana de Recerca i Estudis Avançats, 08010, Barcelona, Spain*
**Corresponding author: joel.villatoro@icfo.es*

Received June 1, 2009; revised July 8, 2009; accepted July 15, 2009;
posted July 21, 2009 (Doc. ID 112105); published August 7, 2009

We report on the fabrication of a monolithic fiber Fabry–Perot interferometer whose cavity is a microscopic air bubble. The latter is formed when splicing together a conventional single-mode fiber and an index-guiding photonic crystal fiber with the standard arc-discharge technique. Spherical microcavities with diameters ranging from 20 to 58 μm were fabricated with such a technique. The interferometers exhibited low thermal sensitivity (less than 1.0 pm/°C), high mechanical strength, broad operation wavelength range, and fringe contrast in the 8–12 dB range. The applications of the interferometers for strain sensing (up to 5000 $\mu\epsilon$) is demonstrated. © 2009 Optical Society of America

OCIS codes: 060.5295, 060.2370.

Fiber optic Fabry–Perot interferometers (FPIs) have proved to be useful for the measurements of diverse physical, chemical, and biological parameters. These interferometers are very sensitive, compact, stable, and reliable. Moreover, their interrogation is relatively simple, which permits the development of high-resolution and versatile sensors. In the past two decades considerable efforts have been made on developing monolithic or intrinsic FPIs. For example, the cavity can be formed within the optical fiber with internal mirrors [1–4]. It can also be carved by means of chemical etching [5–7] or femtosecond laser micromaching [8–10]. Another alternative consists of splicing a short section of hollow core or photonic band gap (PBG) fiber between standard fibers [11–15]. Some drawbacks of the interferometers fabricated with the aforementioned techniques are: multiple steps involved in the fabrication process, surface imperfections caused by the removal of material, low mechanical strength, need of special splicing programs, etc. These drawbacks in general compromise the performance and robustness of the interferometers.

Here we propose a microscopic FPI whose cavity is an air bubble that is formed by splicing together an index-guiding photonic crystal fiber (PCF) and a conventional single-mode fiber (SMF). The splicing of the fibers was carried out with the standard arc-discharge technique. The default programs for splicing SMFs of a commercial splicer (Ericsson FSU 995FA) were used to warranty robust devices and to minimize the fabrication time. A homemade PCF consisting of 2.3 μm diameter air holes arranged in a hexagonal pattern around the core was used [16]. The external diameter of the PCF was 125 μm to simplify the alignment with the SMF. The cross section of the PCF and the diagram of the interrogation setup are shown in Fig. 1.

The splicing of SMFs with different types of PCFs has been studied in the past owing to its relevance; see, for example, [17,18]. During the splicing the fiber ends are typically heated above the softening point for a short period of time by an electric discharge or laser beam. Then the fibers are pressed together to form a permanent joint. Since PCFs have many microscopic holes in the cladding their softening point is in general lower than that of all-solid SMFs. Thus, if a PCF is spliced with an SMF by means of a default splicing program set for monomode fibers, the temperature achieved during the arc discharge will be high enough to exceed the PCF softening point. Under these conditions the surface tension will overcome the viscosity and cause the PCF's air holes to collapse completely over a length of a few hundred micrometers [16–18]. As a result, part of the air originally inside the voids can be trapped, thus forming a microbubble. The shape of the latter is by nature spherical, since the internal pressure is isotropically. The position of the microbubble will be at the center of the fiber if the voids in the PCF are symmetrically distributed.

The predefined program for splicing SMFs was used to fabricate a collection of samples; with this program the cavity was formed in ~90% of the samples, and the diameter of the bubbles was in the 20–25 μm range. The interference patterns observed were regular and stable in most cases with modulation or fringe contrast in the 8–12 dB range. Varia-

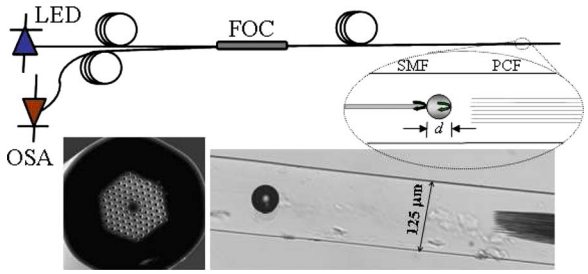

Fig. 1. (Color online) Diagram of the interrogation setup highlighting the zone of the splice. LED, light-emitting diode; OSA, optical spectrum analyzer, FOC, fiber optic circulator; SMF, single-mode fiber; PCF, photonic crystal fiber. d is the diameter of the microcavity. The cross section of the PCF and a micrograph of the splice showing the microbubble are also shown.

tions in the cavity diameter or modulation are probably caused by irregularities in our homemade PCF. We believe that with commercial PCFs better results can be obtained. We would like to point out that when the cleave angle was larger than 1° (measured with the splicing machine) the bubble was not formed, thus indicating that the cleaving is crucial. Also, by modifying the splicing program slightly, cavities with larger diameters, up 58 μm, were fabricated but with less repeatability. Note that in some applications larger cavities can compromise the mechanical strength of the devices.

It is important to point out that the formation of the cavity with the method presented here is carried out with minimal steps that are not time consuming. Once the fibers are cleaved, they are spliced by operating the splicing machine in automatic mode. The technique allows the fabrication of spherical bubbles (cavities) inside the fiber without compromising the mechanical strength of the interferometers. In Fig. 1 a micrograph of a 58 μm diameter bubble is shown. The micrograph of the bubble was taken by immersing the fiber in index-matching oil. Note the spherical shape of the cavity and its precise alignment with the fiber core. The image also shows part of the voids of the PCF.

The air microbubble has two smooth interfaces separated by a distance d (diameter of the bubble). The reflectivity of each glass–air interface is less than 4%. Under these conditions higher-order reflections are negligible, and the device can be considered as a two-beam interferometer. The phase difference ($\Delta\beta$) of the two backreflections is $\Delta\beta = 4\pi nd/\lambda$, with n being the refractive index of the medium trapped inside the bubble and λ being the wavelength of the optical source. The reflected light intensity is $I = I_1 + I_2 + 2\sqrt{I_1 I_2}\cos(\gamma)$, where I_1 and I_2 are the intensities of the beams reflected from the cavity interfaces and γ is the total phase shift. The later is given by $\gamma = \Delta\beta + \pi + \varphi_0$, with φ_0 being an initial phase, and π is added because one reflection takes place from a lower-index–higher-index interface. Thus the reflected spectrum will change periodically with wavelength. The fringe spacing or period of the interference pattern is given by $\Lambda = \lambda^2/(2nd)$. Since the medium inside the cavity is air ($n \approx 1$), then the period depends solely on the size of the microbubble and λ. Figure 2 shows the reflection spectrum over 250 nm observed in a sample with a 58 μm diameter bubble. Note the regular interference pattern and the high fringe contrast. The average fringe spacing observed in two wavelength windows (1300 and 1550 nm) in samples with different diameters of the cavity is also shown in the figure.

The phase of our FPI can change if it is perturbed by environmental variables; consequently, the interferometer can be used for optical sensing. Phase changes can result, for example, in a shift of the interference pattern, which is easy to quantify. Let us analyze first the effect of temperature on the device. Because of thermal expansions of the optical fiber the length of the microbubble can vary with temperature. However, the changes of n (cavity index) are negligible even for high temperatures [13]. We studied the temperature dependence of some devices in the 22°C–500°C range; some results are summarized in Fig. 3. For example, the thermal sensitivity of a sample with $d = 22$ μm was found to be ~0.95 pm/°C. Such sensitivity is extremely low; it is 1 order of magnitude lower than that of the popular fiber Bragg grating (~12 pm/°C).

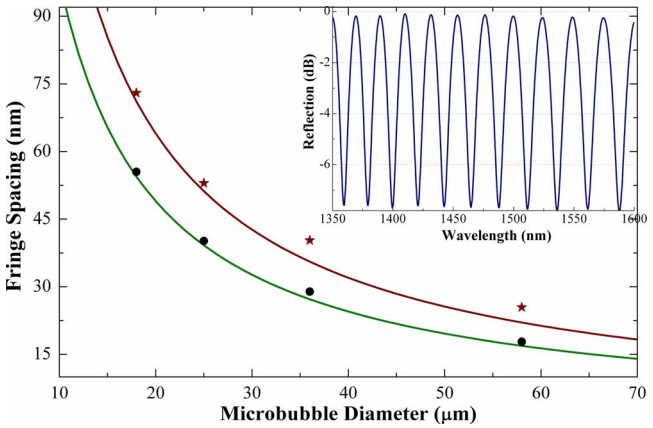

Fig. 2. (Color online) Period as a function of the diameter of the microcavity measured at 1245–1345 (dots) and 1500–1600 (stars) nm wavelength range. The solid curves are fittings to the data. The inset shows the reflection spectrum over 250 nm of an interferometer with a cavity of 58 μm.

Let us now consider that the diameter of the microbubble changes by $\delta d (\ll d)$, which can be caused, for example, by axial strain applied to the interferometer. This effect will change $\Delta\varphi$ and consequently the interference pattern will shift. Since the refractive index of the medium inside the bubble does not change with strain then the shift depends solely on the diameter of the cavity. We investigated the applications of the interferometers as strain sensors. To do so we secured the devices between two linear translation stages and applied/removed axial strain to them [16]. The elongation and compressing processes were repeated several times to verify the sensor reversibility. Figure 4 shows the shift observed as

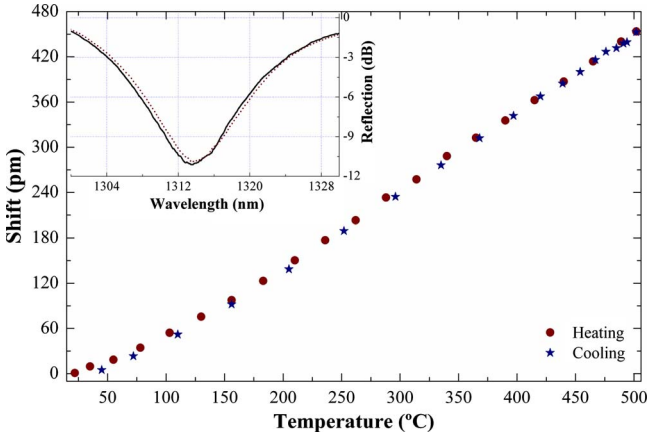

Fig. 3. (Color online) Shift of the interference pattern observed in the 1245–1345 nm wavelength range as a function of temperature. The device had a cavity of $d = 22$ μm. The inset shows the shift of one of the interference dips at 22°C (solid curve) and 500°C (dotted curve).

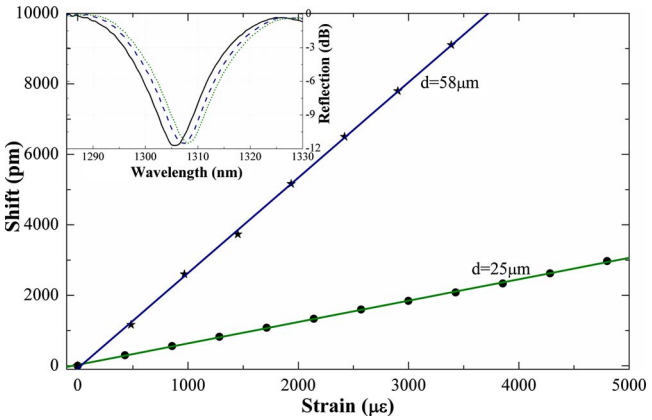

Fig. 4. (Color online) Shift of the interference pattern as a function of strain observed in a 26 μm sample at 1290±40 and in a 58 μm sample at 1550±30 nm. The continuous linear lines are fitting to the data. The inset shows the shift of one of the interference dips at 0 (solid curve), 2570 (dashed curve), and 4288 $\mu\epsilon$ (dotted curve) of the 26 μm sample.

a function of strain in two samples. The 25 μm diameter bubble was subjected to strain ranging from 0 to 5000 $\mu\epsilon$, and the observation was carried out at 1290±40 nm. The 58 μm diameter bubble was also subjected to the same strain range, but the shift was measured at 1550±30 nm. The linear fitting revealed correlation factors of $R^2=0.9991$ and $R^2=0.9994$, respectively. The strain sensitivity of the interferometer with the smaller cavity was 0.62 pm/$\mu\epsilon$, while that of the interferometer with the larger cavity was 2.7 pm/$\mu\epsilon$. The sensitivity in the latter case is about 250% higher than that of FBG-based strain sensors (typically 1.2 pm/$\mu\epsilon$) and comparable with that of more complex PCF-based strain sensors [16]. As strain sensors the PCF enabled micro-FPIs reported here exhibit between four to five times wider dynamic ranges than those based on hollow-core or PBG fibers [8,12,14,15]. On the other hand, the cavities are around ten-times shorter than those of FPIs built with such fibers [8,12,14]. Index-guiding PCFs, therefore, may allow the fabrication of more compact and more robust FPI-based microsensors.

In conclusion, we have reported on the fabrication of miniature monolithic Fabry–Perot-like interferometers. The cavity of such interferometers is a microbubble that is formed by splicing together conventional SMFs and PCFs. The formation of the cavity is carried out with minimal steps and can be monitored *in situ* and in real time with a simple interrogation setup. It was found that the interferometers exhibited low-temperature sensitivity (less than 1 pm/°C). As a potential application of the interferometer strain sensing was demonstrated, but other sensors are envisaged, since many physical parameters can be translated to strain. These sensors can be important in space-constrained applications with the advantage that temperature compensation may not be required.

The authors are grateful to the Spanish Ministerio de Educación y Ciencia and the Ministry of Public Works for funding through the "Ramón y Cajal" program and the project SOPROMAC No. P41/08, respectively. The authors are also grateful to Vladimir P. Minkovich for providing the PCF.

References

1. C. E. Lee, R. A. Atkins, and H. F. Taylor, Opt. Lett. **13**, 1038 (1988).
2. C. E. Lee, W. N. Gibler, R. A. Atkins, and H. F. Taylor, J. Lightwave Technol. **10**, 1376 (1992).
3. X. Wan and H. F. Taylor, Opt. Lett. **27**, 1388 (2002).
4. Z. Huang, Y. Zhu, X. Chen, and A. Wang, IEEE Photon. Technol. Lett. **17**, 2403 (2005).
5. X. Chen, F. Shen, Z. Wang, Z. Huang, and A. Wang, Appl. Opt. **45**, 7760 (2006).
6. V. R. Machavaram, R. A. Badcock, and G. F. Fernando, Sens. Actuators A **138**, 248 (2007).
7. E. Cibula and D. Donlagic, Opt. Express **15**, 8719 (2007).
8. Y. J. Rao, M. Deng, D. W. Duan, X. C. Yang, T. Zhu, and G. H. Cheng, Opt. Express **15**, 14123 (2007).
9. Z. L. Ran, Y. J. Rao, W. J. Liu, X. Liao, and K. S. Chiang, Opt. Express **16**, 2252 (2008).
10. T. Wei, Y. Han, Y. Li, H.-L. Tsai, and H. Xiao, Opt. Express **16**, 5764 (2008).
11. J. S. Sirkis, D. D. Brennan, M. A. Putman, T. A. Berkoff, A. D. Kersey, and E. J. Friebele, Opt. Lett. **18**, 1973 (1993).
12. Y. J. Rao, T. Zhu, X. C. Yang, and D. W. Duan, Opt. Lett. **32**, 2662 (2007).
13. H. Y. Choi, K. S. Park, S. J. Park, U. C. Paek, B. H. Lee, and E. S. Choi, Opt. Lett. **33**, 2455 (2008).
14. Q. Shi, F. Lv, Z. Wang, L. Jin, J. J. Hu, Z. Liu, G. Kai, and X. Dong, IEEE Photon. Technol. Lett. **20**, 237 (2008).
15. E. Li, G. D. Peng, and X. Ding, Appl. Phys. Lett. **92**, 101117 (2008).
16. J. Villatoro, V. Finazzi, V. P. Minkovich, V. Pruneri, and G. Badenes, Appl. Phys. Lett. **91**, 091109 (2007).
17. J. H. Chong and M. Rao, Opt. Express **11**, 1365 (2003).
18. L. Xiao, M. S. Demokan, W. Jin, Y. Wang, and C.-L. Zhao, J. Lightwave Technol. **25**, 3563 (2007).